LETTERS
https://doi.org/10.1038/s41564-020-0719-8

nature microbiology

Check for updates

Competition for iron drives phytopathogen control by natural rhizosphere microbiomes

Shaohua Gu[1], Zhong Wei[1]✉, Zhengying Shao[1], Ville-Petri Friman[1,2], Kehao Cao[1], Tianjie Yang[1], Jos Kramer[3,4], Xiaofang Wang[1], Mei Li[1], Xinlan Mei[1], Yangchun Xu[1]✉, Qirong Shen[1], Rolf Kümmerli[3,4] and Alexandre Jousset[1,5]

Plant pathogenic bacteria cause high crop and economic losses to human societies[1–3]. Infections by such pathogens are challenging to control as they often arise through complex interactions between plants, pathogens and the plant microbiome[4,5]. Experimental studies of this natural ecosystem at the microbiome-wide scale are rare, and consequently we have a poor understanding of how the taxonomic and functional microbiome composition and the resulting ecological interactions affect pathogen growth and disease outbreak. Here, we combine DNA-based soil microbiome analysis with in vitro and in planta bioassays to show that competition for iron via secreted siderophore molecules is a good predictor of microbe–pathogen interactions and plant protection. We examined the ability of 2,150 individual bacterial members of 80 rhizosphere microbiomes, covering all major phylogenetic lineages, to suppress the bacterium *Ralstonia solanacearum*, a global phytopathogen capable of infecting various crops[6,7]. We found that secreted siderophores altered microbiome–pathogen interactions from complete pathogen suppression to strong facilitation. Rhizosphere microbiome members with growth-inhibitory siderophores could often suppress the pathogen in vitro as well as in natural and greenhouse soils, and protect tomato plants from infection. Conversely, rhizosphere microbiome members with growth-promotive siderophores were often inferior in competition and facilitated plant infection by the pathogen. Because siderophores are a chemically diverse group of molecules, with each siderophore type relying on a compatible receptor for iron uptake[8–12], our results suggest that pathogen-suppressive microbiome members produce siderophores that the pathogen cannot use. Our study establishes a causal mechanistic link between microbiome-level competition for iron and plant protection and opens promising avenues to use siderophore-mediated interactions as a tool for microbiome engineering and pathogen control.

Soil-borne pathogens are a global threat to food production[1–3]. Apart from the damage they inflict, a main problem is that there are very few management strategies available to control soil-borne bacterial phytopathogens. Plant root-associated microbiomes are increasingly seen as a possible driver of natural pathogen resistance and have become a target for innovative strategies aiming at improving crop protection[13–15]. However, our ability to predict and engineer microbiome function is still very limited and past research splits into two disjointed lines. The first line of studies has used comparative approaches to unravel how the microbiome structure and the prevalence of putatively pathogen-suppressive traits correlate with plant health[13,16,17]. The second line has focused on specific systems to mechanistically test whether factors such as antibiosis, resource competition and activation of plant immunity can affect plant protection[18–20]. Although the former line reveals potentially important candidate traits, species or functions involved in pathogen suppression, it provides limited insights on the underlying causal mechanisms. Conversely, the latter line offers specific mechanistic insights but it is often difficult to generalize the results beyond the specific study system. As a result, it remains largely unclear which bacterial taxa and what type of ecological interactions in the rhizosphere determine disease outcomes by soil-borne pathogens[21].

We combined the two above-mentioned lines of research to create a predictive framework applicable for disease outcomes for tomato rhizosphere microbiomes: we first taxonomically characterized 80 tomato rhizosphere microbiomes and then conducted experimental analysis using 2,150 representative bacterial members of these microbiomes. In particular, we assessed the interaction of each isolate with the pathogen *Ralstonia solanacearum* (strain QL-Rs1115)—an economically important global pathogen that causes damage to more than 200 plants species[6,7]—both in vitro and in vivo in controlled greenhouse experiments using tomato plants. We then closed the loop by using in vitro interactions as an inference tool to explain covariation in species co-occurrence under natural settings. We hypothesized that competition for iron, through the secretion of siderophores that scavenge iron from the environment, could represent a universal mechanism determining to what extent members of the soil microbiome can suppress the pathogen and protect plants. Although other mechanisms, including resource competition or antibiosis, are probably also involved in bacterial interactions, we reasoned that these mechanisms might be superseded by competition for iron due to its universal importance for bacterial growth. Our reasoning is based on recent studies indicating that siderophore-mediated competition for iron drives eco-evolutionary dynamics in natural and infectious settings[22–25]. Iron is an essential cofactor for many enzymes, yet its bioavailability is low in most soils, because iron predominantly occurs in its insoluble ferric Fe(III) form[26–28]. Many bacteria scavenge iron from the environment through the secretion of siderophores,

[1]Jiangsu Provincial Key Lab for Organic Solid Waste Utilization, Jiangsu Collaborative Innovation Center for Solid Organic Waste Resource Utilization, National Engineering Research Center for Organic-based Fertilizers, Nanjing Agricultural University, Nanjing, P R China. [2]Department of Biology, University of York, York, UK. [3]Department of Quantitative Biomedicine, University of Zurich, Zurich, Switzerland. [4]Department of Plant and Microbial Biology, University of Zurich, Zurich, Switzerland. [5]Institute of Environmental Biology, Ecology and Biodiversity, Utrecht University, Utrecht, The Netherlands. ✉e-mail: weizhong@njau.edu.cn; ycxu@njau.edu.cn

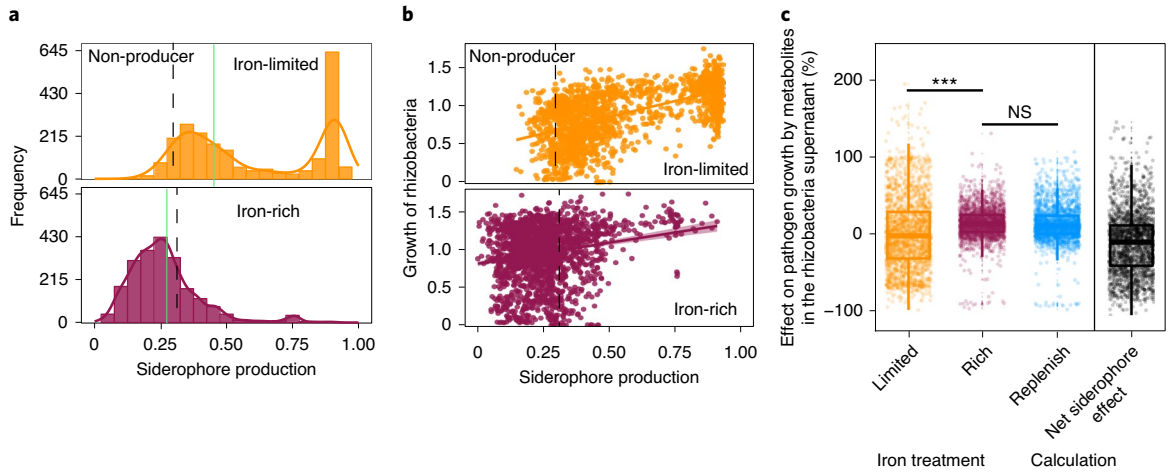

Fig. 1 | Siderophore production by rhizosphere bacteria and their growth effects on the plant pathogenic *R. solanacearum* bacterium. a, Relative siderophore production of the 2,150 rhizosphere isolates (measured in culture supernatants using the CAS assay) under iron-limited (top) and iron-rich (bottom) conditions. The black dashed vertical lines show the average CAS background values measured in the supernatants of two defined siderophore-deficient mutants (non-producers). We used this cut-off line to distinguish background noise from siderophore production. Measuring CAS background is important because this assay also measures the activity of other organic iron-binding compounds in the supernatant. Furthermore, the cut-off can vary slightly between species and the media from which the supernatants were collected (see also Extended Data Fig. 2). The green vertical lines represent siderophore production of our model pathogen *R. solanacearum* strain QL-Rs1115 (CAS value = 0.462 in iron-limited medium). **b**, Siderophore production (measured as CAS activity) across all isolates significantly correlated with rhizosphere bacterial growth (determined as the optical density (OD) at 600 nm, OD_{600}) under iron-limited conditions (top), indicating that siderophores are important for growth. This effect was much weaker under iron-rich conditions (bottom). The black dashed vertical lines show the background CAS assay values of defined siderophore non-producers, the yellow and purple lines and the shaded area depict the best-fit trendlines and the 95% confidence interval of the linear regression, respectively. Regression model for iron-limited condition (top): adjusted $R^2 = 0.388$, $F_{1,1248} = 1{,}362$ and two-sided $P < 2.2 \times 10^{-16}$; iron-rich condition (bottom): adjusted $R^2 = 0.039$, $F_{1,1248} = 87.7$ and two-sided $P < 2.2 \times 10^{-16}$ based on a Student's *t*-test; $n = 2{,}150$ biologically independent rhizobacterial isolates for both. **c**, The growth effects were measured in supernatants collected under iron-limited (high siderophore concentration + other secreted metabolites), iron-rich (low siderophore concentration + other secreted metabolites) and iron-limited conditions replenished with iron (siderophore effect removed, while the effect of other metabolites is retained). The net effect caused by siderophores alone (right column) was obtained by subtracting the growth effect of the iron-replenished supernatant from the growth effect of the iron-limited supernatant. The values indicate the percentage fold-change in growth. The box plots encompass the 25–75th percentiles, the whiskers extend to the minimum and maximum points, and the midline indicates the median ($n = 2{,}150$ biologically independent rhizobacterial isolates). $P < 2.2 \times 10^{-16}$ (left) and $P = 0.882$ (right) based on an analysis of variance followed by a paired two-sided Student's *t*-test. ***$P < 0.001$; NS, not significant.

a chemically diverse group of secondary metabolites with a high affinity for iron[23,29]. The uptake of iron through iron-loaded siderophores occurs via strain-specific receptors, and siderophores can both facilitate and suppress competitors, depending on whether competitors possess the matching receptors for siderophore uptake[8–12].

To assess the role of iron competition within the microbiome for plant protection, we first characterized 80 tomato rhizosphere microbiomes (Extended Data Fig. 1a) collected from four different fields in China (Supplementary Table 1), which were all infected by *R. solanacearum*. The main phyla of these microbiomes included Proteobacteria (28%), Bacteroidetes (18%), Planctomycetes (9%), Patescibacteria (8%), Actinobacteria (6%), Acidobacteria (6%) and Firmicutes (4%); 293 families and 756 genera in total. We then randomly isolated and characterized a collection of 2,150 culturable bacteria, which covered four major phylogenetic lineages normally present in plant rhizospheres[30] and were also present in our soil microbiomes (Proteobacteria (50%), Firmicutes (24%), Bacteroidetes (18%) and Actinobacteria (8%); 35 families and 83 genera in total; Extended Data Fig. 1b). This collection is thus partly representative of the taxonomic breath of our soil microbiomes.

We then used the coulometric chrome azurol S (CAS) assay to estimate the levels of secreted siderophores in the supernatant of all 2,150 bacterial isolates. This assay serves as a proxy for siderophore production and revealed that up to 95% of the isolates produced siderophores, given that their CAS values exceeded the ones of siderophore-deficient control strains (Fig. 1a,b). Estimating background CAS values is important, as this assay also measures the binding activities of other organic iron-binding compounds. When the CAS assay was repeated under iron-rich conditions, we found that up to 99% of the siderophore producers upregulated siderophore production under iron-limited conditions compared with iron-rich conditions (Extended Data Fig. 2). Under iron limitation, siderophore production followed a bimodal distribution with isolates producing either high or low quantities of siderophores (Fig. 1a). Siderophore production (that is, CAS activity) across all isolates was predictive of bacterial growth under iron-limited conditions (coefficient of determination (R^2) = 0.388, $n = 2{,}150$; Fig. 1b) but barely had an effect under iron-rich condition ($R^2 = 0.039$, $n = 2{,}150$; Fig. 1b). These results suggest that siderophore production is a widespread trait across the taxa and sampling sites examined here and is important for bacterial growth under iron-limited conditions.

We then assessed the potential of the siderophores from the different isolates to suppress or promote the growth of *R. solanacearum* (QL-Rs1115). We first applied a baseline treatment by feeding bacterial supernatants collected from iron-rich conditions, which contained few siderophores but presumably other secreted compounds and residual nutrients, to the pathogen. We found that these supernatants had a mild and overall significant stimulatory effect on the growth of *R. solanacearum* (Fig. 1c and Extended Data Fig. 3a). Conversely, when the pathogen received bacte-

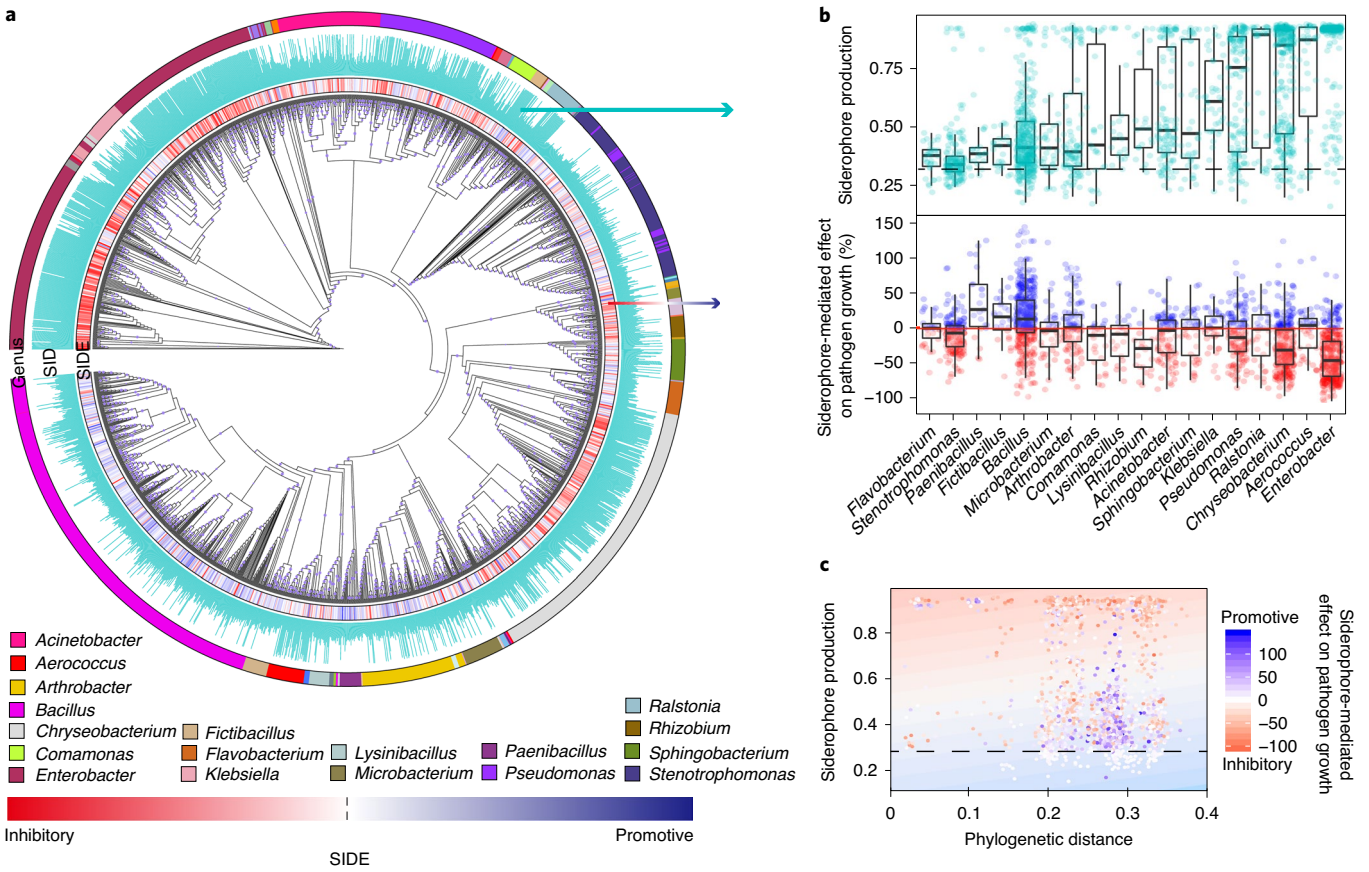

Fig. 2 | The taxon identity of the rhizobacterial isolates and their phylogenetic distance to *R. solanacearum* affect the siderophore-mediated growth effects on the pathogen. a, Cladogram depicting the phylogenetic relationship among the 2,150 isolates based on the 16S rRNA gene sequences. The first inner ring depicts the siderophore-mediated growth effects on the pathogen as a heatmap ranging from red (inhibitory) to blue (promotive), the second ring shows relative siderophore production by each isolate and the outer ring shows the most abundant genera (number of isolates greater than 20). SIDE, siderophore-mediated effect on pathogen growth; SID, siderophore production. **b**, Variation among isolates of the 18 most prevalent genera with regard to siderophore production (top) and siderophore-mediated effect on pathogen growth (bottom). The black dashed line shows the background CAS assay values of siderophore non-producers under iron-limited conditions. Values above and below the red line represent siderophore-mediated promotive and inhibitory effects of rhizobacteria on the pathogen growth. The exact number of bacteria in each genus is shown in Supplementary Table 7. The box plots encompass the 25–75th percentiles, the whiskers extend to the minimum and maximum points, and the midline indicates the median. **c**, Relationship between the siderophore-mediated effect on pathogen growth, phylogenetic distance between the pathogen and rhizosphere bacteria, and siderophore production in iron-limited conditions. This relationship explained a high proportion of the observed variance (25.6%) in iron-limited conditions (visualized as a heatmap based on the generalized linear model analysis, background). The dotted lines represent the background CAS assay values of defined siderophore non-producers. Each point represents one of the 2,150 isolates and its colour shade indicates the strength of the siderophore-mediated effect on pathogen growth (adjusted $R^2 = 0.255$, $F_{1,1248} = 87.7$ and two-sided $P < 2.2 \times 10^{-16}$ based on Student's *t*-tests for the whole model).

rial supernatants from iron-limited conditions—which contained larger quantities of siderophores—we found the effects on growth to be substantially more pronounced (Fig. 1c and Extended Data Fig. 3a). These effects ranged from almost complete suppression of *R. solanacearum* growth to high levels of pathogen facilitation. To validate whether the observed differences in growth effects between the iron-rich and iron-limited conditions were indeed caused by siderophores and not by other secreted metabolites that might have been up- or downregulated under iron limitation, we exposed the pathogen to iron-limited supernatants that were replenished with iron to repress iron competition. The addition of iron to these supernatants neutralizes the effect of siderophores but retains the effect of the other secreted metabolites (for example, antibiotics) on pathogen growth. We found that iron-replenished supernatants had the same (mildly promotive) effects as iron-rich supernatants, suggesting that siderophores are the main drivers of bacterial interactions under iron-limited conditions. When estimating the net effect of siderophores (Fig. 1c) we indeed found that siderophores explained 76% of the total supernatant-mediated growth effects on *R. solanacearum* ($R^2 = 0.755$, $n = 2{,}150$, $P < 0.0001$; Fig. 1c and Extended Data Fig. 3b).

To experimentally confirm that siderophores can drive bacteria–pathogen interactions, we grew *R. solanacearum* in the presence of iron-limited supernatants from two defined siderophore producers (*Pseudomonas aeruginosa* PAO1 producing pyoverdine and pyochelin; *Burkholderia cenocepacia* H111 producing ornibactin and pyochelin) and their isogenic null mutants, which were unable to produce siderophores due to engineered deletions of siderophore-synthesis genes (Extended Data Fig. 3c). We found that the supernatants of the wild-type strains (containing siderophores) showed pathogen growth inhibition. Conversely, these inhibitory effects completely disappeared when the pathogen was exposed to the supernatants from the siderophore-deficient isogenic mutants of the two species (Extended Data Fig. 3c). To further confirm the importance of siderophores in mediating inter-species interactions, we isolated and purified the pyoverdines

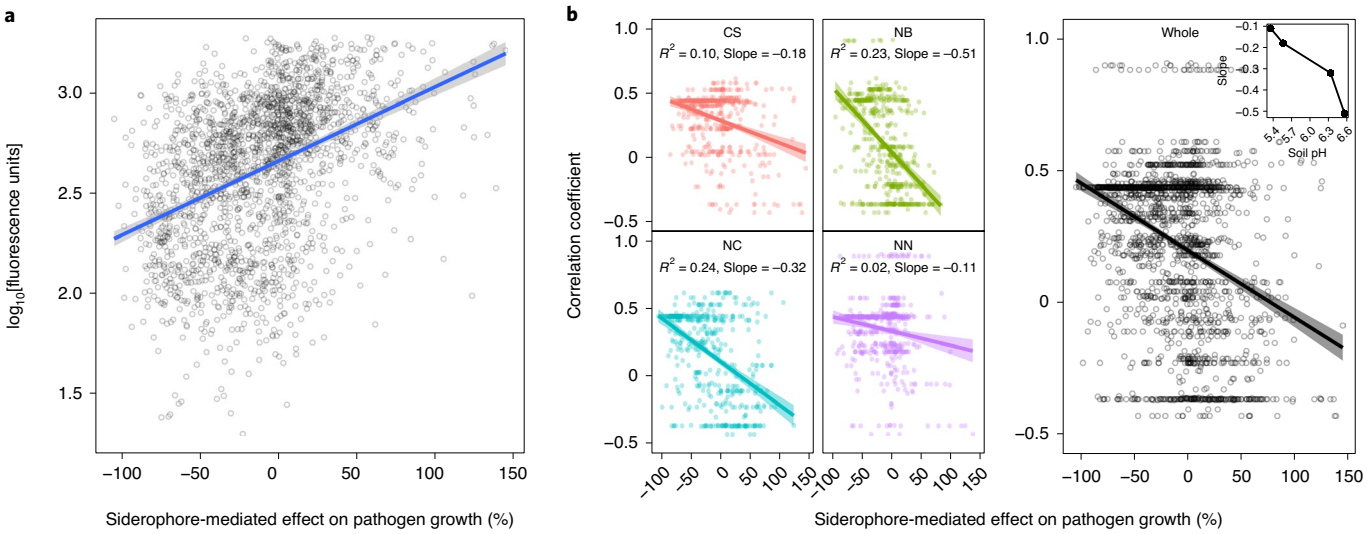

Fig. 3 | Siderophore-mediated effects on pathogen growth correlate with *R. solanacearum* and rhizosphere bacterial abundances in vitro and in vivo under field conditions. a, Co-culture experiments between the *R. solanacearum* pathogen and each of the 2,150 rhizosphere isolates show that pathogen density (measured as mCherry fluorescence units) correlates positively with siderophore-mediated growth effects, suggesting that siderophores determine pathogen growth when in direct competition with rhizosphere bacteria. The blue line and grey shaded area depict the best-fit trendline and the 95% confidence interval of the linear regression, respectively (adjusted $R^2 = 0.16$, $n = 2{,}150$ biologically independent rhizobacterial isolates, $F_{1,1248} = 404.6$ and two-sided $P < 2.2 \times 10^{-16}$ based on a Student's *t*-test). **b**, Co-occurrence between the pathogen and rhizosphere bacteria was estimated as the correlation coefficient across the 80 soil samples and plotted against the effect of siderophores on pathogen growth. Exclusively negative correlations were found between these variables, showing that rhizosphere bacteria producing inhibitory siderophores tended to coexist at high densities with the pathogen (positive *r*), whereas isolates producing promotive siderophores tended to occur at low densities when the pathogen was abundant (negative *r*). Inset, the strength of this relationship correlated with the soil pH at the four sampling sites (right). Left, the colours represent different sampling sites: CS, Changsha ($n = 528$ biologically independent rhizobacterial isolates, $F_{1,526} = 58.72$, $P < 2.2 \times 10^{-16}$); NB, Ningbo ($n = 526$ biologically independent rhizobacterial isolates, $F_{1,524} = 154.1$, $P < 2.2 \times 10^{-16}$); NC, Nanchang ($n = 508$ biologically independent rhizobacterial isolates, $F_{1,506} = 157.1$, $P < 2.2 \times 10^{-16}$); NN, Nanning ($n = 568$ biologically independent rhizobacterial isolates, $F_{1,566} = 14.9$, $P = 0.0001$). The results of linear regression analysis in the left panel are shown as colour-coded best-fit trendlines for each sampling site (the shaded areas depict the 95% confidence interval and adjusted R^2 with the slope of the best-fit trendlines). Right, adjusted $R^2 = 0.133$ and the shaded area depicting the 95% confidence interval are shown ($n = 2{,}130$ biologically independent rhizobacterial isolates, $F_{1,1228} = 272.7$ and two-sided $P < 2.2 \times 10^{-16}$ based on Student's *t*-tests for the whole data across four sampling sites).

of four different *Pseudomonas* spp. isolates and exposed the pathogen to these siderophores. We observed that all four siderophores inhibited pathogen growth under iron-limited conditions in a similar way to the iron-limited supernatants (Extended Data Fig. 3d). Finally, we examined the growth and siderophore production of *R. solanacearum* QL-Rs1115 in monoculture. We found that the pathogen is constrained in its growth in our iron-limited medium (Extended Data Fig. 4a), upregulates siderophore production under iron limitation to an intermediate level (CAS-value = 0.462; Fig. 1a and Extended Data Fig. 4b) and is growth-stimulated when supplemented with its own iron-limited supernatant containing siderophores (Extended Data Fig. 4c). Together, these results demonstrate that siderophores can play a key role in mediating interactions between rhizosphere isolates and *R. solanacearum* QL-Rs1115 under iron-limited conditions. They further suggest that the promotion or inhibition of siderophore-mediated growth is indicative of whether *R. solanacearum* has compatible or incompatible receptors for heterologous siderophore uptake, respectively, as has been described for other bacterial taxa[12,22].

We next examined whether bacterial taxonomic affiliations predict siderophore production and siderophore-mediated effects on the pathogen. We observed a significant phylogenetic signal[31] for both traits (Abouheif's $C_{mean} = 0.262$ (siderophore production) and 0.148 (siderophore-mediated growth effects); $P < 0.001$ for both traits), which were relatively weak ($C_{mean} = 1$ would mean that all the observed variation is explained by phylogeny). This indicates that both siderophore production and siderophore-mediated growth effects vary substantially between related isolates, possibly due to a recent change, gain or loss of trait functions. This assertion is supported by our ancestral character state reconstruction analysis showing that high levels of siderophore production and siderophore-mediated growth effects evolved independently multiple times (Supplementary Fig. 1). A focused analysis on the 18 most common genera confirms that both common ancestry and differences within genera contribute to trait variation (Fig. 2b): (1) certain genera clearly differ from one another in their siderophore production and the extent to which they affect *R. solanacearum* growth (for example, compare *Enterobacter* versus *Bacillus*) and (2) there is high variation between isolates within genera in the two traits (for example, *Bacillus* spp.).

At the quantitative level, we found that the inhibition of *R. solanacearum* growth was predicted by the additive effects of phylogenetic distance and siderophore production, with the most inhibiting isolates being those that were relatively closely related to the pathogen and that produced high quantities of siderophores (Fig. 2c; whole model $R^2 = 0.255$, $n = 2{,}150$; Supplementary Table 2). This phylogenetic effect is consistent with the ecological theory predicting that resource competition intensifies among more closely related species, as their ecological niches are more likely to overlap[32,33]. To validate the effect between the level of siderophore production and the siderophore-mediated growth effect, we repeated our analysis using phylogenetically independent contrasts, thereby filtering out the variation explained by phylogeny alone. This analysis confirmed that isolates producing high quantities of siderophores were more likely to inhibit *R. solanacearum* growth than isolates producing low quantities of siderophores (Extended Data Fig. 5).

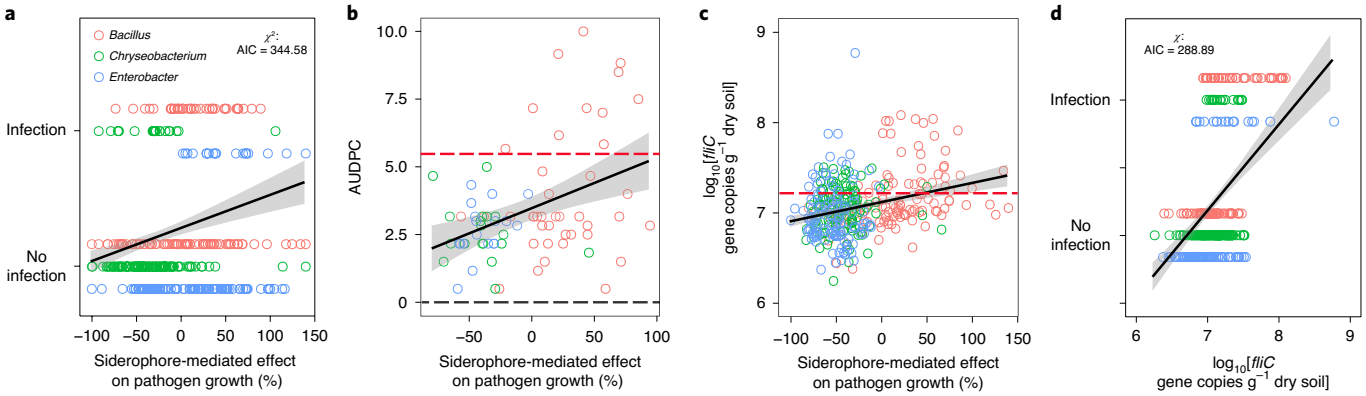

Fig. 4 | Siderophore-mediated growth effects predict plant disease outcomes and pathogen load in the tomato plant rhizosphere during greenhouse experiments. a, The ability of pathogens to infect tomato plants was measured as a binary variable for each of the 360 pathogen–bacteria combinations; infection was scored as successful if at least one of six plants was infected. Successful infection scaled positively with the effect of siderophores on pathogen growth, suggesting that inhibitory siderophores can protect plants from infections ($n = 360$ biologically independent rhizobacterial isolates and two-sided $P = 4.85 \times 10^{-8}$ based on a χ^2 test). **b**, Disease severity of infected plants (quantified as the area under disease progress curve, AUDPC) correlated positively with the siderophore-mediated growth effect on the pathogen. For this analysis, we only considered the 77 isolates that actually managed to infect plants (adjusted $R^2 = 0.149$, $n = 77$ biologically independent rhizobacterial isolates, $F_{1,75} = 14.34$ and two-sided $P = 0.0003$ based on a Student's *t*-test). **c**, Pathogen densities correlated positively with the siderophore-mediated growth effect on the pathogen, suggesting that the sign of siderophore-mediated effects determine pathogen load in the tomato rhizosphere (adjusted $R^2 = 0.105$, $n = 360$ biologically independent rhizobacterial isolates, $F_{1,358} = 42.92$ and two-sided $P = 6.16 \times 10^{-9}$ based on a Student's *t*-test). **b**,**c**, The red and black dashed lines show the baseline values for the control treatments in which the tomato plants were inoculated with either *R. solanacearum* alone or sterilized water, respectively. **d**, Successful infection scaled positively with pathogen densities, suggesting that successful inhibition of pathogen growth is key for disease control ($n = 360$ biologically independent rhizobacterial isolates and two-sided $P = 2.31 \times 10^{-13}$ based on a χ^2 test). **a**–**d**, The black lines and grey shaded areas depict the best-fit trendline and the 95% confidence interval of the logistic regression, respectively. AIC, Akaike information criterion.

We then examined whether the siderophore-mediated growth effects can predict the outcome of direct competition between each of the 2,150 rhizosphere isolates and *R. solanacearum* in co-cultures. We found that pathogen growth was significantly reduced when competing against taxa producing inhibitory siderophores ($R^2 = 0.16$, $n = 2{,}150$; Fig. 3a). To test whether the siderophore-mediated growth effects correlate with patterns of co-occurrence between the pathogen and rhizosphere bacteria in natural field conditions, we used 16S rDNA sequencing of the whole microbiome communities and quantitative PCR (qPCR) to estimate the co-occurrence patterns of each taxon with the pathogen in each of the 80 soil samples. Thus, we obtained the prevalence of the pathogen and the 2,150 taxa for each microbiome. We then correlated these prevalence values across the 80 microbiomes. We found that siderophore-mediated interactions correlated with species co-occurrence in the field: taxa producing inhibitory siderophores tended to co-occur with the pathogen at high density (positive regression coefficient, *r*), whereas taxa producing promotive siderophores tended to occur at low densities when the pathogen was abundant (negative *r*, main effect of in vivo coexistence on *r* with $R^2 = 0.113$, $n = 2{,}150$, Fig. 3b). These patterns of covariance were strongest at the sites with high soil pH values (Fig. 3b, inset and Supplementary Table 3), where iron availability is most reduced and siderophores most needed (Fig. 3b, inset). Although many other (unknown) factors can influence the abundance of taxa in the field, our results indicate that siderophore-mediated interactions can be a generalizable mechanism that substantially influences the competitive outcomes and the co-occurrence patterns between the pathogen and taxa isolated from natural rhizosphere microbiomes. Moreover, the power of siderophores to predict species interactions seems to vary with environmental parameters, such as pH, that directly influence the level of iron limitation in soils, and we propose that other environmental factors, such as overall iron content and nutrient availability, could have similar effects.

Finally, we tested whether the siderophore-mediated interactions can affect the ability of the pathogen to invade the rhizosphere microbiome and cause disease, using tomato plants that were individually pre-colonized by one of 360 randomly selected bacterial isolates belonging to the three most abundant genera (*Bacillus*, on average promotive; *Enterobacter*, on average inhibitory; and *Chryseobacterium*, on average inhibitory; 120 isolates tested per genus; Supplementary Table 4). We found that the siderophore-mediated interactions were significantly associated with both pathogen growth and plant protection (Fig. 4). Specifically, disease incidence and pathogen density were highest when the pre-inoculated bacterial isolates produced promotive siderophores but decreased when the plants were pre-inoculated with bacteria producing inhibitory siderophores (Fig. 4a–c and Extended Data Fig. 6). Crucially, the siderophore-mediated effects on the infection outcomes were not dependent on the genus (see Supplementary Table 5 for the statistical analysis). Moreover, pathogen density correlated positively with disease incidence (Fig. 4d), suggesting that inhibition of pathogen growth plays a key role in disease control. Although the associations reported here are all significant, it is important to realize that they only explain a relatively low level of the total variation observed. This suggests that in addition to siderophores, other factors also influence the infection outcomes. Together, our infection experiments match the growth and co-occurrence patterns observed (both in vitro and in the field) well, indicating that siderophore-mediated interactions provide a substantial contribution towards and reliably predict pathogen suppression and disease outcomes in many cases.

In conclusion, our study links global microbiome analyses with high-throughput experimental assays to demonstrate that siderophore-mediated interactions are an overarching mechanism influencing microbiome function in natural field conditions. Our findings set the stage for microbiome-wide ecosystem engineering to suppress pathogens and protect crops. A key component of

microbiome engineering or the development of probiotics would be to selectively promote the members of the microbiome with siderophore-inhibitory effects on the pathogen and reduce those with pathogen-promotive siderophores. Great care should be taken to choose species that produce siderophores that cannot be taken up by the pathogen. Our study has identified groups of soil bacteria with such preferable functions; the next step would be to genetically and chemically identify the pathogen-suppressive and -promotive siderophores. The types of siderophores produced by all of the members of the microbiome could form a database against which the siderophore types of any pathogenic bacteria could be mapped to identify the specific members of the microbiome with incompatible siderophores. We propose that such siderophore mismatch analyses could represent a predictive tool for microbiome-mediated pathogen management. An important aspect of such an approach would be to include measures to minimize the risk of resistance evolution by pathogens—for example, through the acquisition of heterologous siderophore receptors through horizontal gene transfer[34]. In this context, it would be important to promote diverse rhizosphere communities that combat the pathogen at multiple fronts, through the secretion of a chemically diverse set of siderophores. It is conceivable that, in a scenario where pathogens are confronted with a cocktail of inhibitory siderophores, resistance cannot easily evolve.

Methods

Rhizosphere soil sampling. Rhizosphere soil samples were collected from individual tomato plants located on four geographically distant fields (Supplementary Table 1) that had suffered from bacterial wilt disease for 3–15 yr: Changsha (112°58′ E, 28°11′ N), Ningbo (121°67′ E, 29°91′ N), Nanchang (115°51′ E, 28°41′ N) and Nanning (108°21′ E, 22°49′ N). Twenty rhizosphere soil samples (20 tomato plants) were collected from each site. To this end, the excess soil was first gently shaken from the roots and the remaining soil attached to the roots was considered as the rhizosphere soil. Each rhizosphere soil sample was then divided into two parts: one to isolate bacteria and the other to extract DNA for bacterial community sequencing and the quantification of *R. solanacearum* pathogen densities using qPCR. The soil pH was measured (as described in a previous study[35]) because low soil pH is positively linked to iron bioavailability in the soil[36].

Soil DNA extraction. The soil DNA was extracted from 300 mg soil using a Power soil DNA isolation kit (MO BIO Laboratories, Inc.) according to the manufacturer's protocol. The DNA quality was checked by running the samples on 1% sodium boric acid agarose gels and the DNA concentrations were measured using a NanoDrop 1000 spectrophotometer (Thermo Scientific). The extracted DNA was stored at −80 °C.

Isolation of rhizobacteria. To isolate bacteria, 1 g rhizosphere soil was mixed with 9 ml MS buffer solution (50 mM Tris–HCl, pH 7.5, 100 mM NaCl, 10 mM $MgSO_4$ and 0.01% gelatin) in a rotary shaker at 170 r.p.m. for 30 min at 30 °C. After serial dilution in MS buffer solution, 100-µl volumes of the diluted soil suspensions were plated on 1/10 tryptone soya agar (1/10 TSA; 1.5 g l^{-1} tryptone, 0.5 g l^{-1} soytone, 0.5 g l^{-1} sodium chloride, and 15 g l^{-1} agar, pH 7.0). After a 48-h incubation at 30 °C in the dark, 32 isolates were randomly picked per rhizosphere soil sample. To avoid potential fungal contamination, only highly diluted samples were used for isolation. The isolates were then re-streaked on TSA plates for colony purification. Approximately 16.0% of the bacterial isolates failed to grow on the TSA plates for unknown reasons and were omitted from the dataset (approximately the same number of isolates failed to grow for each field). The final collection consisted of 2,150 bacterial isolates from 80 rhizosphere soil samples. All purified isolates were cultured in 100 µl tryptone soya broth (TSB, liquid TSA) on 96-well microtitre plates at 30 °C with shaking (rotary shaker at 170 r.p.m.) for 18 h before freezing and storing at −80 °C in 15% glycerol.

16S ribosomal RNA gene sequencing of rhizobacteria. We used 16S rRNA amplicon sequencing to taxonomically identify all 2,150 rhizobacterial isolates. Total genomic DNA was extracted from overnight cultures of the individual bacterial isolates, cultured in TSB medium at 30 °C with shaking (170 r.p.m.), using an E.Z.N.A. bacterial DNA kit (OMEGA Bio-tek) following the manufacturer's protocol. The 16S rRNA gene was amplified by PCR using the universal primers F27 (5′-AGAGTTTGATCATGGCTCAG-3′) and R1492 (5′-TACGGTTACCTTGTTACGACTT-3′)[37]. The PCR reactions (25 µl) contained 1 µl bacterial DNA, 12.5 µl master mix, 1 µl each of the forward and reverse primers, and 9.5 µl deionized water. The PCR was run as follows: initial denaturation at 95 °C for 5 min, 30 cycles of denaturation at 94 °C for 30 s, annealing at 58 °C for 30 s, extension at 72 °C for 1 min 30 and the final extension at 72 °C for 10 min. The PCR products were sequenced by Shaihai Songon Biotechnology Co., Ltd. The 16S rDNA sequences were identified using the NCBI and RDP databases and homologous sequence similarity. To incorporate pairwise phylogenetic distance between the pathogen and each isolate as a covariate into models, the relatedness between the rhizobacterial isolates and the pathogen was calculated using pairwise alignment of 16S rDNA sequences using EMBOSS Water[38].

Tree construction and phylogenetic analysis of rhizobacterial isolates. To construct and explore the phylogenetic relationships between the rhizobacterial isolates and the pathogen, the 16S rDNA sequences of all strains (2,150) were aligned using MUSCLE. The sequences in the alignment were trimmed at both ends to obtain maximum overlap using the MEGA 7 software, which was also used to construct taxonomic cladograms and calculate the phylogenetic distances between rhizobacteria and the pathogen[39]. We constructed a maximum-likelihood tree using a General time reversible + G + I model, which yielded the best fit to our dataset. Bootstrapping was carried out with 100 replicates retaining the gaps. The taxonomic cladogram was created using the iTOL web tool (http://huttenhower.sph.harvard.edu/galaxy/). To allow for further phylogenetic analyses, the tree was midpoint-rooted, multichotomies were randomly resolved into a series of dichotomies and a small constant (10^{-6} times the maximum branch length) was added to branches with a length of zero. We first used the revised tree to calculate the phylogenetic signal (Abouheif's C_{mean})[31] in the production of siderophores and the siderophore-mediate effects on pathogen growth, using the phyloSignal function of the phylosignal package[40] in R. We then performed an ancestral character estimation of these two traits. Finally, we compared the results of a correlation based on the uncorrected trait values with the results of a correlation based on phylogenetically independent contrasts to test for an effect of phylogeny on the association between siderophore production and siderophore-mediated effects on pathogen growth. Both analyses (ancestral character estimation and calculation of phylogenetically independent contrasts) were performed with the ape package[41], using the ace (which fits a Brownian motion model by residual maximum likelihood) and pic functions, respectively.

Measuring the growth of rhizobacteria and their siderophore production. To quantify the growth and siderophore production of each rhizobacterial isolate under iron-limited and iron-rich conditions, we first revived the isolates by transferring 5-µl volumes of their respective freezer stocks into new 96-well plate containing 195 µl TSB per well and then cultured the bacteria overnight at 30 °C with shaking (rotary shaker set at 170 r.p.m.). We then transferred 10 µl of the overnight cultures into new 96-well plates containing 190 µl MKB medium (2.5 g l^{-1} K_2HPO_4, 2.5 g l^{-1} $MgSO_4 \cdot 7H_2O$, 15 ml l^{-1} glycerin and 5.0 g l^{-1} casamino acids, pH 7.2). This medium contains low quantities of residual iron[42] but still allows all of the isolates to grow to a certain extent regardless of their ability to produce siderophores (Fig. 1b). As an iron-rich control medium, we supplemented MKB with 50 µM $FeCl_3$. We selected a high concentration of iron to ensure that iron is no longer a limiting factor for the growth of all of the isolates examined. Following a 48-h incubation at 30 °C with shaking (rotary shaker set at 170 r.p.m.), we measured the bacterial growth as the maximum density obtained with a plate reader at room temperature (OD_{600}; SpectraMax M5).

The same samples were then used to quantify the rhizobacterial siderophore production. Specifically, we harvested the cell-free supernatant from bacterial cultures by centrifugation (4,000 r.p.m., 5 min at 4 °C) and filtration (using a 0.22 µm filter). The supernatant was then divided into two parts to measure the siderophore production and test the supernatant effects on *R. solanacearum* pathogen growth. Siderophore production was assayed using a modified version of the universal chemical assay developed by Schwyn and Neilands[43]. Briefly, we used the liquid version of the CAS assay, where 100 µl cell-free supernatant (three biological replicates for all 2,150 soil isolates) or deionized water as a control reference were added to 100 µl CAS assay solution in a 96-well plate. After 2 h of static incubation at room temperature, the OD_{630} of the cell-free supernatants (A) and deionized water controls (Ar) was then measured using a plate reader (SpectraMax M5) at room temperature. Siderophores induce a colour change in the CAS medium, which lowers the OD_{630} measurements, and siderophore production can thus be quantified using the following formula: $1 - A \div Ar$. Because media components (that is, organic acids) and other secreted compounds can also bind iron, it is essential to estimate the CAS signal background that is not due to siderophores. We assessed this signal background using defined siderophore-deficient mutants from two species (*P. aeruginosa* PAO1Δ*pvdD*Δ*pchEF* and *B. cenocepacia* H111Δ*orbJ*Δ*pchAB*)[44,45] and their corresponding wild types using the same protocol as described above. We then averaged the CAS background signals of the two siderophore-deficient mutants and used it as a cut-off line to distinguish siderophore producers from non-producers among our 2,150 soil isolates.

Effect of rhizobacterial supernatants on the growth of *R. solanacearum*. We used the *R. solanacearum* strain QL-Rs1115 tagged with the pYC12–mCherry plasmid[16] as a model pathogen. To explore the interactions between this pathogen and the 2,150 members of the rhizosphere microbiomes via secreted products

(overview of the experimental design is shown in Supplementary Fig. 2), we exposed the pathogen to three different types of supernatant collected from the rhizobacteria. These treatments included: (1) supernatants collected from iron-rich conditions (rhizobacteria grown in iron-rich MKB medium, in which few siderophores are produced but other compounds are secreted; SN_{ri}), (2) supernatants collected from iron-limited conditions (rhizobacteria grown in iron-limited MKB medium, which triggers siderophore production in addition to other secreted compounds; SN_{li}) and (3) supernatants collected from iron-limited conditions that were subsequently replenished with 50 µM $FeCl_3$ (SN_{re}). This supernatant still contains siderophores but they are no longer relevant for iron uptake, as the iron is available in excess. As a control, we used sterilized water instead of supernatant ($SN_{control}$). All supernatant assays were carried out in triplicate. Specifically, we inoculated 2 µl of an overnight culture of the pathogen (adjusted to $OD_{600} = 0.5$ after 12 h growth at 30 °C with shaking) into 180 µl fresh MKB medium (10× dilution to better reflect the effect of the supernatant) and 20 µl sterile rhizobacterial supernatant. The cultures were then incubated at 30 °C with shaking (rotary shaker set at 170 r.p.m.). Pathogen growth was measured as the OD_{600} (SpectraMax M5 plate reader) after 24 h of cultivation. We subsequently calculated the effect of the rhizobacterial supernatant on pathogen growth relative to growth in the absence of supernatants using the following formula: growth effect $GE_{treatment} = ((SN_{treatment} \div SN_{control}) - 1) \times 100$, where $SN_{treatment}$ is SN_{li}, SN_{ri} or SN_{re}. For this calculation, we took the average supernatant effects across the three replicates. Values smaller and greater than zero indicate growth inhibition and facilitation, respectively, expressed as the percentage fold-change in growth. From these measures, the net GE of siderophores can be measured as $GE_{net} = GE_{li} - GE_{re}$.

Control experiments to test whether foreign siderophores affect the growth of *R. solanacearum*. We performed two control experiments to validate that foreign siderophores affect pathogen growth as shown by the supernatant assays. First, we used the same protocol as described earlier to obtain iron-limited supernatants (in triplicate) from two defined siderophore producers (*P. aeruginosa* PAO1 and *B. cenocepacia* H111) and their isogenic null mutants, which are unable to produce siderophores due to engineered deletions of siderophore-synthesis genes (PAO1Δ*pvdD*Δ*pchEF* and H111Δ*orbJ*Δ*pchAB*)[44,45]. We then followed the protocol described earlier to challenge the pathogen with these supernatants to test whether inhibition of pathogen growth occurs only with supernatants from the wild-type strains and not with the supernatants from the siderophore-deficient strains.

In a second control experiment, we extracted and purified the siderophores (pyoverdines) from four *Pseudomonas* isolates in our isolate collection (Supplementary Table 6). These four isolates produce large quantities of pyoverdine, which can be detected via the natural fluorescence of this molecule (relative fluorescence units measured with an excitation at 400 nm and emission at 460 nm), using a microplate reader[12]. We first revived the four isolates by transferring 5 µl of their respective freezer stocks into 25-ml conical flasks containing 10 ml TSB, and cultured the bacteria overnight at 30 °C with shaking (rotary shaker set at 170 r.p.m.). We then transferred 1 ml of the overnight cultures into 250-ml conical flasks containing 100 ml iron-limited medium (MKB). Following a 48-h incubation at 30 °C (with shaking at 170 r.p.m.), we extracted the pyoverdines in the supernatants using a standardized method[12,46]. We then dissolved the purified pyoverdines in 10 ml deionized water and passed it through a filter (0.22 µm) for sterilization. Finally, the sterile pyoverdine solutions were used to assess their effect on pathogen growth under iron-limited conditions using the same protocol that was used for the supernatant assay.

Control experiments examining the impact of iron limitation on the growth and siderophore production of *R. solanacearum* QL-Rs1115. We carried out three additional control experiments to verify that the pathogen *R. solanacearum* QL-Rs1115 itself is limited by iron in the MKB medium, produces siderophores under iron-limiting conditions and is stimulated by its own iron-limited supernatant containing siderophores. We found all these points held true (Extended Data Fig. 4). Before performing these experiments, we inoculated *R. solanacearum* from freezer stocks into 200 µl TSB medium to grow overnight at 30 °C in 96-well microplates. We then transferred 10 µl of the overnight cultures into new 96-well plates containing 200 µl of one of three media (five replicates): (1) MKB medium supplemented with 50 µM $FeCl_3$ (high iron availability), (2) MKB medium (low iron availability) and (3) MKB medium supplemented with 200 µM 2,2′-dipyridyl, a strong iron chelator (very low iron availability). Following a 48-h incubation at 30 °C with shaking at 170 r.p.m., we measured the pathogen growth through absorbance at OD_{600} using a plate reader (SpectraMax M5).

We then used the cultures from the iron-limited (MKB) and iron-rich (MKB + iron) medium to collect sterile supernatants, for which we quantified the siderophore contents using the CAS assay as per the protocol described earlier. Finally, we repeated the supernatant growth assay as reported in Fig. 1c, but this time we provided *R. solanacearum* with its own supernatants. We did this to test whether the pathogen is stimulated by its own siderophores, which are present in the iron-limited but not the iron-rich and iron-replenished supernatants.

Control experiment testing whether mCherry fluorescence remains stable across a pH gradient. We observed that the pH of the MKB medium rises from 7.17 to 7.55 during a 24-h growth cycle of *R. solanacearum*. As we aimed to use the mCherry signal as a proxy for pathogen growth in mixed cultures with the rhizosphere isolates, we tested whether the mCherry fluorescence measurements remained stable across a pH range of 6 to 10. Specifically, we took cultures of *R. solanacearum* in the stationary phase and adjusted the pH to 6 (with dilute hydrochloric acid) and 10 (with sodium hydroxide solution). After allowing the bacterial cultures to adjust to the new pH for 1 h, we quantified the mCherry fluorescence of the original culture (unmanipulated pH) and the pH-adjusted bacterial cultures (excitation, 587 nm and emission, 610 nm) using the SpectraMax M5 plate reader. We found that the mCherry fluorescence intensity was not significantly affected by the pH of the bacterial cultures (Supplementary Fig. 3).

Effect of rhizobacteria on pathogen growth in the co-cultures. We co-cultured each rhizobacterial isolate with the pathogen in the iron-limited MKB medium that triggers siderophore production to test whether the siderophores produced by rhizobacteria affect pathogen growth directly. To this end, we first cultured all rhizobacterial isolates and *R. solanacearum* pathogens from 5 µl of their respective freezer stocks overnight at 30 °C in 96-well microplates containing 200 µl of TSB medium. We then co-cultured each rhizobacteria with the pathogen by mixing 10 µl of both overnight cultures into new 96-well plates containing 200 µl iron-limited MKB medium at 30 °C with shaking (170 r.p.m.). After 24 h, we quantified the pathogen density on the basis of the constitutively expressed mCherry fluorescence signal (excitation at 587 nm and emission at 610 nm) using a SpectraMax M5 plate reader. To control for the auto-fluorescence of rhizobacteria, we also grew each isolate as a monoculture in iron-limited MKB medium and subtracted these monoculture values from the co-culture fluorescence values. This allowed us to correlate the changes in pathogen density with the siderophore-mediated growth effect of each pathogen-rhizobacterial isolate pair.

Quantification of *R. solanacearum* densities in the field with qPCR. The density of *R. solanacearum* in the fields was determined using qPCR with primers targeting the *fliC* gene, which encodes a flagellar subunit (forward primer, 5′-GAACGCC AACGGTGCGAACT-3′ and reverse primer, 5′-GGCGGCCTTCAGGGAG GTC-3′)[47]. The qPCR was carried out using an Applied Biosystems 7500 real-time PCR system. We used SYBR Green I fluorescent dye detection in 20-µl volumes containing 10 µl SYBR premix Ex Taq (TaKaRa Bio Inc.), 2 µl DNA template extracted from rhizosphere soil and 0.4 µl of both the forward and reverse primers (10 mM each). The qPCR was performed with an initial denaturing step of 30 s at 95 °C, with subsequent cycling (40×) with a 5 s denaturing step at 95 °C. The protocol was followed by a 34 s elongation/extension step at 60 °C, and a melt curve analysis for 15 s at 95 °C followed by 1 min at 60 °C and finally for 15 s at 95 °C. Melt curves were obtained based on a standard protocol and used to identify the characteristic peak of PCR product (400 bp)[48]. Three independent technical replicates were used for each sample.

Estimation of the diversity and relative bacterial abundances in the field with 16S rRNA amplicon sequencing. To determine the relative abundance of rhizobacterial isolates in the field, we first sequenced the whole bacterial communities of the 80 tomato rhizosphere samples by amplifying the V4 hypervariable regions of the bacterial 16S rRNA gene using the primer pair 563F (5′-AYTGGGYDTAAAGVG-3′) and 802R (5′-TACNVGGGTATCTAATCC-3′)[49]. The PCR reactions (total volume of 20 µl) contained 4 µl 5×Fast-Pfu buffer, 2 µl 2.5 mM dNTPs, 0.4 µl of each primer (5 µM), 0.5 µl DNA sample and 0.4 µl Fast-Pfu polymerase (TransGen Biotech). The PCR amplification was conducted using an Applied Biosystems thermal cycler (GeneAmp PCR system 9700) and included 30 cycles at 95 °C for 30 s, 55 °C for 30 s and 72 °C for 30 s. Three independent PCRs were performed for each DNA sample and the triplicate products were pooled to minimize PCR amplification bias. The amplicon products were purified using an AxyPrep PCR clean-up kit (Axygen Biosciences) and the sample purities were verified by agarose gel electrophoresis. The concentrations of the purified PCR products were determined using QuantiFluor-ST (Promega) before subjecting them to 250-nucleotide paired-end sequencing on an Illumina MiSeq platform at Shanghai Biozeron Biotechnology Co., Ltd. The sequence data were processed following the UPARSE pipeline[50]. Briefly, read pairs from each sample were assembled, low-quality nucleotides (maximal expected error of 0.25) were removed and reads shorter than 200 bp were discarded. After the elimination of singletons and chimeras using the UCHIME method[51], sequence depth of 30,071–44,756 reads were attained for all samples. The soil-sample sequences were then clustered using the 16S rDNA sequences of the 2,150 culturable rhizobacteria as reference taxa based on a 97% similarity threshold. The relative abundance of each identified taxa cluster was then calculated as the percentage of clustered reads of the total sequence reads (30,071–44,756 reads, which also included sequences that did not match the 2,150 culturable isolates) and analysed using QIIME[52]. As we did not find matching sequences for 20 of the culturable bacterial isolates, these bacterial isolates were removed from further analysis.

Determining the rhizobacteria–pathogen co-abundances in the field. We further tested whether the siderophore-mediated growth effects could explain the co-abundance patterns between the rhizobacteria and *R. solanacearum* pathogen

in the field. To this end, we combined the pathogen qPCR and rhizobacterial 16S rRNA data and correlated the pathogen densities with the relative abundance of each rhizobacteria across all of the 80 tomato rhizosphere samples, resulting in 2,150 regression coefficients. Positive coefficients indicate that pathogen densities are high when the rhizobacterial abundances are also high, whereas negative coefficients indicate that pathogen densities are low when the rhizobacterial abundances are high. We then correlated these regression coefficients with siderophore-mediated growth effects on the pathogen.

Establishing a causal link between siderophore-mediated growth inhibition and reduced pathogenicity in the tomato rhizosphere. We carried out a 60-d-long greenhouse experiment to test whether siderophore-mediated growth inhibition in the rhizosphere reduces the incidence of bacterial wilt disease in tomatoes. For this experiment, we randomly selected 360 rhizobacteria belonging to the three most-abundant genera (120 isolates from *Enterobacter*, *Bacillus* and *Chryseobacterium* taxa each). As the iron-limited supernatants from *Bacillus* had both inhibitory (approximately one-third of all isolates) and promotive effects (approximately two-thirds of all isolates), we randomly picked 40 and 80 isolates belonging to the two respective categories. We grew tomato seedlings in six-well trays filled with growth substrate (100 g substrate per well; commercially available from Jiangsu-Xingnong Substrate Technology Co., Ltd), which was sterilized with gamma radiation before experimentation. Surface-sterilized tomato seeds (*Lycopersicon esculentum*, cultivar 'Micro-Tom') were germinated on water-agar plates for 3 d before sowing into six-well trays. At the three-leaf stage, six plants were independently inoculated with one of the 360 rhizobacterial isolates at a final concentration of 1×10^8 colony-forming units (CFU) g^{-1} of substrate[53] (total of 2,172 plants). One week later, *R. solanacearum* was introduced to the roots of all plants at a final concentration of 1×10^7 CFU g^{-1} of substrate. In addition, we had two control treatments—that is, tomato plants treated with only the *R. solanacearum* (no rhizobacteria) or sterilized water (no rhizobacteria or pathogen). All plants were grown in a greenhouse with a natural temperature variation range of 25 to 35 °C and were watered regularly with sterile water. The seedling trays were randomly rearranged every 3 d. Disease progression was monitored every second day after the first disease symptoms appeared. The incidence of plant disease was later quantified as the AUDPC[54] based on disease incidence (percentage of wilted plants), which is frequently used to combine multiple observations of disease progress into a combined single value. The greenhouse experiment was finished 40 d following the inoculation with *R. solanacearum*, after which we pooled the rhizosphere soil from the six plant replicates, extracted the bacterial DNA and quantified the *R. solanacearum* densities using the qPCR protocol described earlier.

Statistical analysis. We used generalized linear models to test whether the production of siderophores and other metabolites affects the growth of rhizobacteria directly (co-cultures) and indirectly (supernatants) in iron-limited and iron-rich conditions in the lab, and the absolute and relative abundances of the pathogen and rhizobacteria in the field. The relationship between phylogenetic distance, siderophore production and the siderophore-mediated effect on pathogen growth were visualized as a heatmap using the R package visreg. Relationships between the pathogen and rhizobacterial abundances with siderophore-mediated effects were analysed using linear regressions. When comparing mean differences between treatments, we used analysis of variance (Duncan's multiple range and Mann–Whitney *U* tests) and Student's *t*-tests where *P* values below 0.05 were considered statistically significant. Generalized linear models were also used to analyse pathogen density and disease incidence data (AUDPC) in the greenhouse experiment. To meet assumptions of normality and homogeneity of variance, data were $\log_{10}$-transformed when required. All statistical analyses were carried out using the R 3.1.2 program (www.r-project.org).

Reporting Summary. Further information on research design is available in the Nature Research Reporting Summary linked to this article.

Data availability

Raw data of the high-throughput sequences of the 80 soil samples (accession numbers SRR8949365–SRR8949444) and sequencing data of the 2,150 strains (accession numbers MK823189–MK825338) can be found in the NCBI database. All source data has been deposited to the Dryad Digital Repository with the following digital identifier: https://doi.org/10.5061/dryad.p8cz8w9mb.

Code availability

All code used in this study are available from the corresponding author on request.

Received: 5 June 2019; Accepted: 3 April 2020;
Published online: 11 May 2020

References

1. Fisher, M. C. et al. Emerging fungal threats to animal, plant and ecosystem health. *Nature* **484**, 186–194 (2012).
2. Anderson, P. K. et al. Emerging infectious diseases of plants: pathogen pollution, climate change and agrotechnology drivers. *Trends Ecol. Evol.* **19**, 535–544 (2004).
3. Savary, S. et al. The global burden of pathogens and pests on major food crops. *Nat. Ecol. Evol.* **3**, 430–439 (2019).
4. Andrews, J. H. & Harris, R. F. The ecology and biogeography of micro-organisms on plant surfaces. *Annu. Rev. Phytopathol.* **38**, 145–180 (2000).
5. Dodds, P. N. & Rathjen, J. P. Plant immunity: towards an integrated view of plant–pathogen interactions. *Nat. Rev. Genet.* **11**, 539–548 (2010).
6. Mansfield, J. et al. Top 10 plant pathogenic bacteria in molecular plant pathology. *Mol. Plant Pathol.* **13**, 614–629 (2012).
7. Poueymiro, M. & Genin, S. Secreted proteins from *Ralstonia solanacearum*: a hundred tricks to kill a plant. *Curr. Opin. Microbiol.* **12**, 44–52 (2009).
8. Niehus, R., Picot, A., Oliveira, N. M., Mitri, S. & Foster, K. R. The evolution of siderophore production as a competitive trait. *Evolution* **71**, 1443–1455 (2017).
9. Bruce, J. B., Cooper, G. A., Chabas, H., West, S. A. & Griffin, A. S. Cheating and resistance to cheating in natural populations of the bacterium *Pseudomonas fluorescens*. *Evolution* **71**, 2484–2495 (2017).
10. Butaite, E., Kramer, J., Wyder, S. & Kummerli, R. Environmental determinants of pyoverdine production, exploitation and competition in natural *Pseudomonas* communities. *Environ. Microbiol.* **20**, 3629–3642 (2018).
11. Smith, E. E., Sims, E. H., Spencer, D. H., Kaul, R. & Olson, M. V. Evidence for diversifying selection at the pyoverdine locus of *Pseudomonas aeruginosa*. *J. Bacteriol.* **187**, 2138–2147 (2005).
12. Butaite, E., Baumgartner, M., Wyder, S. & Kummerli, R. Siderophore cheating and cheating resistance shape competition for iron in soil and freshwater *Pseudomonas* communities. *Nat. Commun.* **8**, 414 (2017).
13. Kwak, M. J. et al. Rhizosphere microbiome structure alters to enable wilt resistance in tomato. *Nat. Biotechnol.* **36**, 1100–1109 (2018).
14. Berendsen, R. L., Pieterse, C. M. & Bakker, P. A. The rhizosphere microbiome and plant health. *Trends Plant Sci.* **17**, 478–486 (2012).
15. Compant, S., Samad, A., Faist, H. & Sessitsch, A. J. A review on the plant microbiome: ecology, functions and emerging trends in microbial application. *J. Adv. Res.* **19**, 29–37 (2019).
16. Wei, Z. et al. Trophic network architecture of root-associated bacterial communities determines pathogen invasion and plant health. *Nat. Commun.* **6**, 8413 (2015).
17. Li, M. et al. Facilitation promotes invasions in plant-associated microbial communities. *Ecol. Lett.* **22**, 149–158 (2019).
18. Pieterse, C. M. et al. Induced systemic resistance by beneficial microbes. *Annu. Rev. Phytopathol.* **52**, 347–375 (2014).
19. van der Meij, A., van Wezel, G. P., Hutchings, M. I. & Worsley, S. F. Chemical ecology of antibiotic production by actinomycetes. *FEMS Microbiol. Rev.* **41**, 392–416 (2017).
20. Casper, B. B. & Jackson, R. B. Plant competition underground. *Annu. Rev. Ecol. Evol. Syst.* **28**, 545–570 (1997).
21. Cordovez, V., Dini-Andreote, F., Carrión, V. J. & Raaijmakers, J. M. Ecology and evolution of plant microbiomes. *Annu. Rev. Microbiol.* **73**, 69–88 (2019).
22. Cordero, O. X., Ventouras, L. A., DeLong, E. F. & Polz, M. F. Public good dynamics drive evolution of iron acquisition strategies in natural bacterioplankton populations. *Proc. Natl Acad. Sci. USA* **109**, 20059–20064 (2012).
23. Kummerli, R., Schiessl, K. T., Waldvogel, T., McNeill, K. & Ackermann, M. Habitat structure and the evolution of diffusible siderophores in bacteria. *Ecol. Lett.* **17**, 1536–1544 (2014).
24. Andersen, S. B., Marvig, R. L., Molin, S., Krogh Johansen, H. & Griffin, A. S. Long-term social dynamics drive loss of function in pathogenic bacteria. *Proc. Natl Acad. Sci. USA* **112**, 10756–10761 (2015).
25. Barber, M. F. & Elde, N. C. Buried treasure: evolutionary perspectives on microbial iron piracy. *Trends Genet.* **31**, 627–636 (2015).
26. Andrews, S. C., Robinson, A. K. & Rodriguez-Quinones, F. Bacterial iron homeostasis. *FEMS Microbiol. Rev.* **27**, 215–237 (2003).
27. Colombo, C., Palumbo, G., He, J.-Z., Pinton, R. & Cesco, S. Review on iron availability in soil: interaction of Fe minerals, plants, and microbes. *J. Soils Sediments* **14**, 538–548 (2014).
28. Miethke, M. & Marahiel, M. A. Siderophore-based iron acquisition and pathogen control. *Microbiol. Mol. Biol. Rev.* **71**, 413–451 (2007).
29. Hider, R. C. & Kong, X. Chemistry and biology of siderophores. *Nat. Prod. Rep.* **27**, 637–657 (2010).
30. Lagos, L. et al. Current overview on the study of bacteria in the rhizosphere by modern molecular techniques: a mini-review. *J. Soil Sci. Plant Nutr.* **15**, 504–523 (2015).
31. Münkemüller, T. et al. How to measure and test phylogenetic signal. *Methods Ecol. Evol.* **3**, 743–756 (2012).
32. Hibbing, M. E., Fuqua, C., Parsek, M. R. & Peterson, S. B. Bacterial competition: surviving and thriving in the microbial jungle. *Nat. Rev. Microbiol.* **8**, 15–25 (2010).
33. Jousset, A., Schmid, B., Scheu, S. & Eisenhauer, N. Genotypic richness and dissimilarity opposingly affect ecosystem functioning. *Ecol. Lett.* **14**, 537–545 (2011).

34. Kramer, J., Özkaya, Ö. & Kümmerli, R. Bacterial siderophores in community and host interactions. *Nat. Rev. Microbiol.* **18**, 152–163 (2019).
35. Schofield, R. K. & Taylor, A. W. The measurement of soil pH. *Soil Sci. Soc. Am. J.* **19**, 164–167 (1955).
36. Loper, J. E. & Henkels, M. D. Availability of iron to *Pseudomonas fluorescens* in rhizosphere and bulk soil evaluated with an ice nucleation reporter gene. *Appl. Environ. Microbiol.* **63**, 99–105 (1997).
37. Heuer, H., Krsek, M., Baker, P., Smalla, K. & Wellington, E. M. Analysis of actinomycete communities by specific amplification of genes encoding 16S rRNA and gel-electrophoretic separation in denaturing gradients. *Appl. Environ. Microbiol.* **63**, 3233–3241 (1997).
38. Tamura, K., Nei, M. & Kumar, S. Prospects for inferring very large phylogenies by using the neighbor-joining method. *Proc. Natl Acad. Sci. USA* **101**, 11030–11035 (2004).
39. Kumar, S., Stecher, G. & Tamura, K. MEGA7: molecular evolutionary genetics analysis version 7.0 for bigger datasets. *Mol. Biol. Evol.* **33**, 1870–1874 (2016).
40. Keck, F., Rimet, F., Bouchez, A. & Franc, A. phylosignal: an R package to measure, test, and explore phylogenetic signal. Ecol. Evol. 6, 2774–2780 (2016).
41. Paradis, E. & Schliep, K. ape 5.0: an environment for modern phylogenetics and evolutionary analyses in R. *Bioinformatics* **35**, 526–528 (2018).
42. Höfte, M., Buysens, S., Koedam, N. & Cornelis, P. Zinc affects siderophore-mediated high affinity iron uptake systems in the rhizosphere *Pseudomonas aeruginosa* 7NSK2. *Biometals* **6**, 85–91 (1993).
43. Schwyn, B. & Neilands, J. Universal chemical assay for the detection and determination of siderophores. *Anal. Biochem.* **160**, 47–56 (1987).
44. Ghysels, B. et al. The *Pseudomonas aeruginosa pirA* gene encodes a second receptor for ferrienterobactin and synthetic catecholate analogues. *FEMS Microbiol. Lett.* **246**, 167–174 (2005).
45. Sathe, S., Mathew, A., Agnoli, K., Eberl, L. & Kümmerli, R. Genetic architecture constrains exploitation of siderophore cooperation in the bacterium *Burkholderia cenocepacia*. *Evol. Lett.* **3**, 610–622 (2019).
46. Meyer, J.-M. et al. Use of siderophores to type pseudomonads: the three *Pseudomonas aeruginosa* pyoverdine systems. *Microbiology* **143**, 35–43 (1997).
47. Schonfeld, J., Heuer, H., Van Elsas, J. D. & Smalla, K. Specific and sensitive detection of *Ralstonia solanacearum* in soil on the basis of PCR amplification of *fliC* fragments. *Appl. Environ. Microbiol.* **69**, 7248–7256 (2003).
48. Chen, Y. et al. A real-time PCR assay for the quantitative detection of *Ralstonia solanacearum* in horticultural soil and plant tissues. *J. Microbiol. Biotech.* **20**, 193–201 (2010).
49. Cardenas, E. et al. Significant association between sulfate-reducing bacteria and uranium-reducing microbial communities as revealed by a combined massively parallel sequencing-indicator species approach. *Appl. Environ. Microbiol.* **76**, 6778–6786 (2010).
50. Edgar, R. C. UPARSE: highly accurate OTU sequences from microbial amplicon reads. *Nat. Methods* **10**, 996–998 (2013).
51. Edgar, R. C., Haas, B. J., Clemente, J. C., Quince, C. & Knight, R. UCHIME improves sensitivity and speed of chimera detection. *Bioinformatics* **27**, 2194–2200 (2011).
52. Caporaso, J. G. et al. QIIME allows analysis of high-throughput community sequencing data. *Nat. Methods* **7**, 335–336 (2010).
53. Wei, Z. et al. Efficacy of *Bacillus*-fortified organic fertiliser in controlling bacterial wilt of tomato in the field. *Appl. Soil Ecol.* **48**, 152–159 (2011).
54. Jeger, M. J. & Viljanen-Rollinson, S. L. H. The use of the area under the disease-progress curve (AUDPC) to assess quantitative disease resistance in crop cultivars. *Theor. Appl. Genet.* **102**, 32–40 (2001).

Acknowledgements

We thank B. Schmid for insightful comments and suggestions for the manuscript and the students in the class of Re131 who graduated in 2017 from Nanjing Agricultural University for their contributions to this work. This research was financially supported by the National Natural Science Foundation of China (grant nos. 41922053 to Z.W., 41807045 to T.Y. and 31972504 to Y.X.) and the Natural Science Foundation of Jiangsu Province (grant nos. BK20180527 to T.Y. and BK20170085 to Z.W.). V.-P.F. is supported by the Wellcome Trust (grant no. 105624) through the Centre for Chronic Diseases and Disorders (C2D2) and Royal Society Research Grants (grant nos. RSG\R1\180213 and CHL\R1\180031) at the University of York. A.J. is supported by the Nederlandse Organisatie voor Wetenschappelijk Onderzoek (grant no. ALW.870.15.050) and the Koninklijke Nederlandse Akademie van Wetenschappen (grant no. 530-5CDP18). R.K. is supported by the Swiss National Science Foundation (grant no. 31003A-182499) and the European Research Council under the grant agreement no. 681295. J.K. is supported by the German Science Foundation (DFG; grant no. KR 5017/2-1).

Author contributions

S.G., Z.W., X.W., M.L. and X.M. performed and analysed most of the experiments in the laboratory, and S.G., Z.S., T.Y. and K.C. performed and analysed most of the experiments in the greenhouse. J.K. performed most of the phylogenetic analysis. Y.X., Q.S., A.J., V.-P.F. and R.K. provided intellectual input and helped to interpret data. S.G., Z.W., A.J., V.-P.F. and R.K. wrote the manuscript. All of the authors discussed the results and commented on the manuscript. Y.X. and Z.W. supervised the study.

Competing interests

The authors declare no competing interests.

Additional information

Extended data is available for this paper at https://doi.org/10.1038/s41564-020-0719-8.

Supplementary information is available for this paper at https://doi.org/10.1038/s41564-020-0719-8.

Correspondence and requests for materials should be addressed to Z.W. or Y.X.

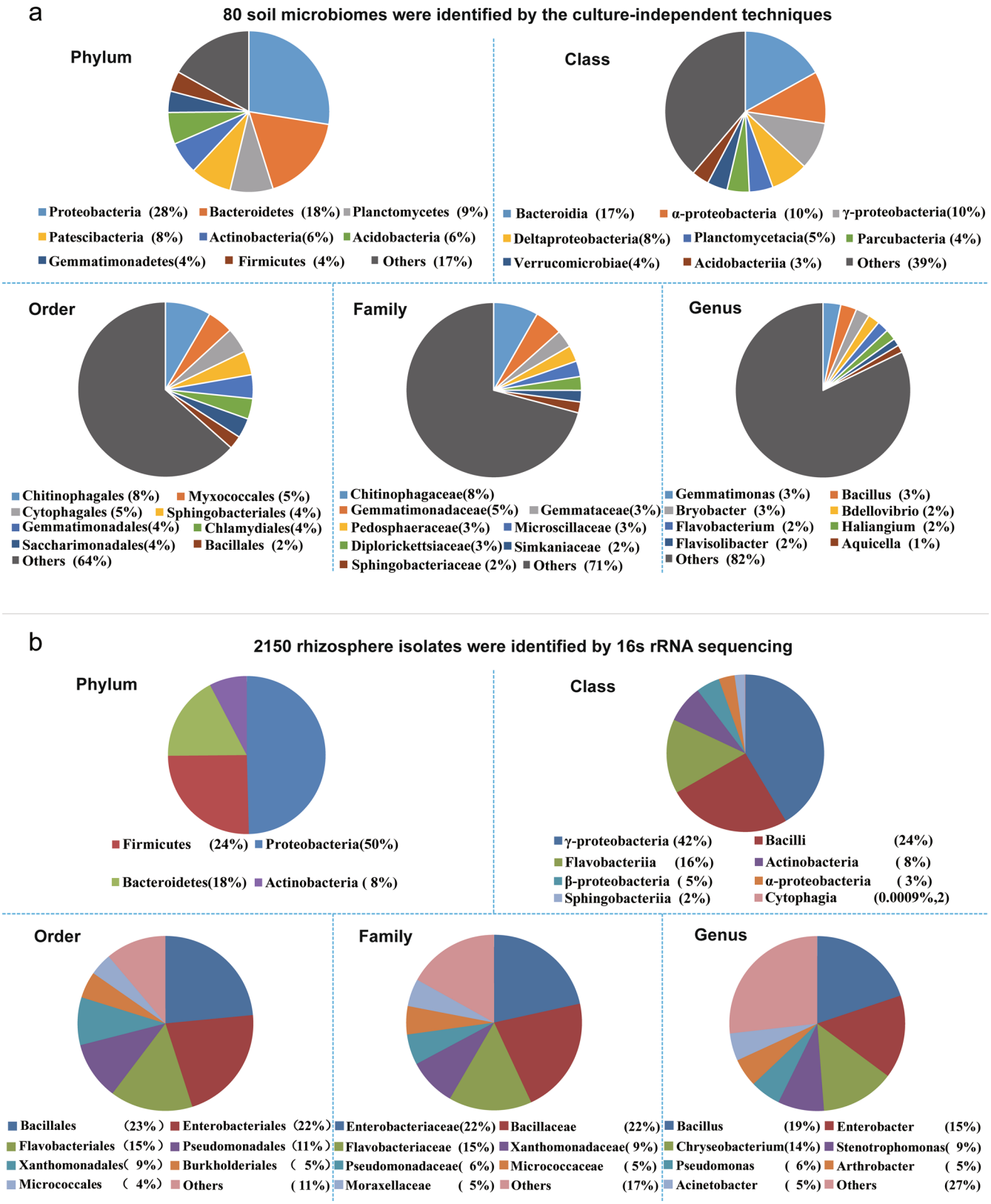

Extended Data Fig. 1 | The diversity and taxonomic classification of rhizosphere microbiomes and bacterial isolates. a, A total of 80 rhizosphere microbiomes were identified by amplifying the V4 hypervariable regions of the bacterial 16S rRNA gene. Eight bacterial groups with highest relative abundances at the phylum, class, order, family, and genus levels are shown in the figure, while groups with relatively low abundances were merged and are presented as one group 'Others'. **b**, A total of 2150 rhizosphere isolates were identified by 16s rRNA sequencing and their closest relatives were determined using the NCBI database. Seven bacterial groups with highest relative abundances at the phylum, class, order, family, and genus levels are shown in the figure, while groups with relatively low abundances were merged and are presented as one group 'Others'. In all panels, percentage (%) values in brackets represent the proportion of each bacterial group of the total OTUs (11929 OTUs; 2150 bacterial isolates).

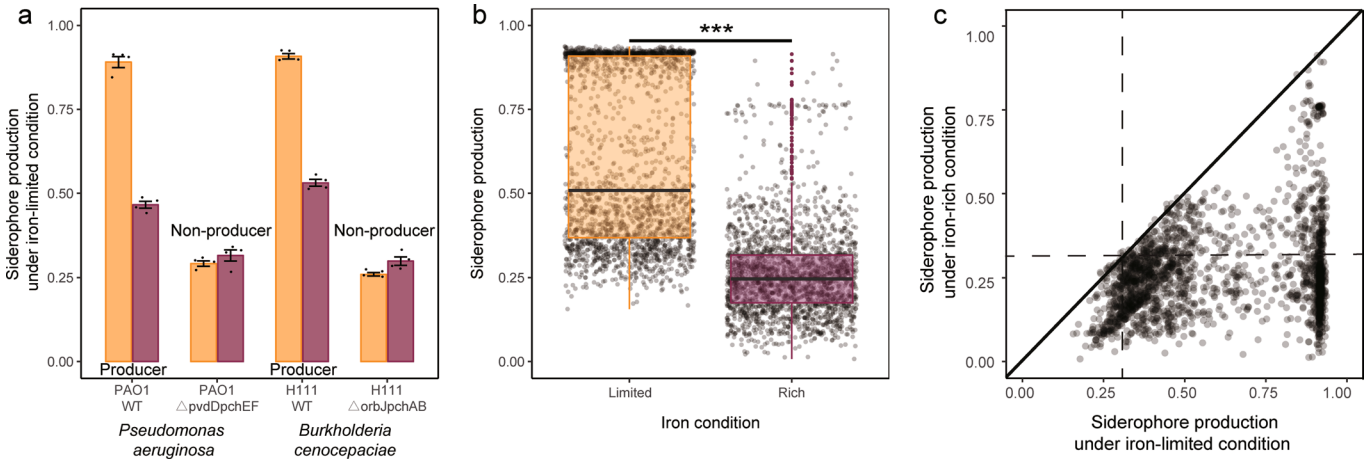

Extended Data Fig. 2 | Siderophore production of defined siderophore producers (WT), their isogenic non-producers (deletion mutants) and the 2,150 rhizosphere isolates. a, CAS values of the two defined wild-type laboratory strains (producer) and the corresponding siderophore-deficient mutants (non-producer) under iron-limited (yellow) and iron-rich (purple) conditions. We used the background CAS values of the siderophore-deficient mutants as a cut-off value to distinguish background CAS activity from siderophore production. Data represent the mean±s.d. of the siderophore production, n=4 independent biological replicates (shown as black dots over the bars). **b**, Mean siderophore production of the 2150 rhizosphere isolates is significantly higher under iron-limited compared to iron-rich conditions. Box plots encompass the 25–75th percentiles, the whiskers extend to the minimum and maximum points and the midline indicates the median (n=2150 biologically independent rhizobacterial isolates. *P* values were determined based on analysis of variance (ANOVA) followed by paired two-sided Student's *t* test. $P<2.2\times10^{-16}$ (*$P < 0.05$, **$P < 0.01$, ***$P < 0.001$)). **c**, Iron limitation induces siderophore production in up to 99% of all siderophore producers (values fall below the solid black line). Data points that fall on the solid black line, *ie*, the diagonal of the square, denotes that equal amount of siderophores were produced under iron-limited and iron-rich conditions. The black dashed lines represent the background CAS values of the two siderophore non-producers under iron-limited and iron-rich conditions, respectively.

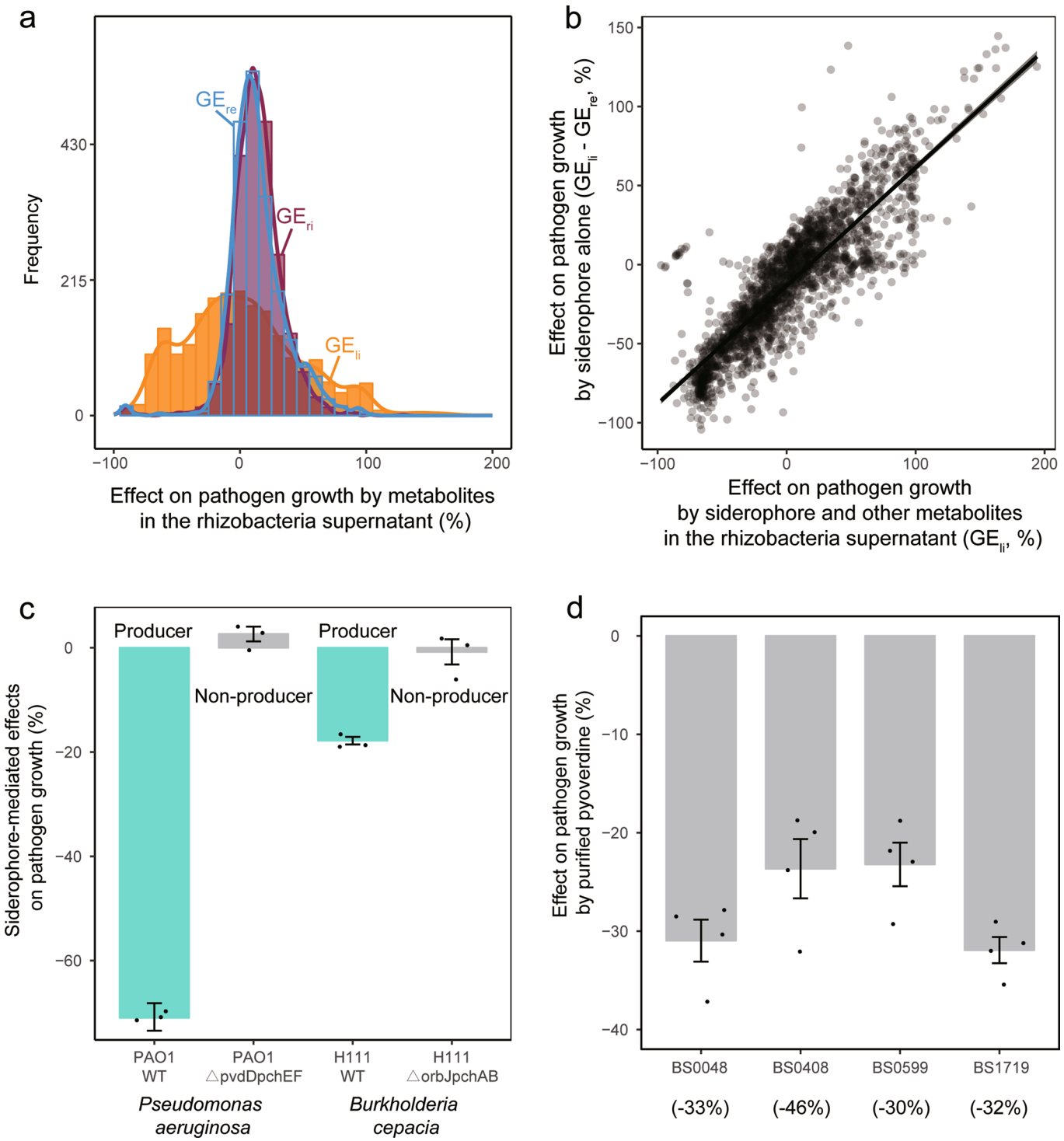

Extended Data Fig. 3 | The growth effects of siderophores by rhizosphere bacteria on the plant pathogenic *R. solanacearum* bacterium. a, The histogram shows how the growth of the pathogen *R. solanacearum* was affected by cell-free rhizobacterial supernatants collected from iron-limited (yellow fit, GE_{li}) and iron-rich (purple fit, GE_{ri}) media, and when iron-limited supernatants were replenished with iron (blue fit, GE_{re}). **b**, The panel contrasts GE_{li} (effects mediated by siderophores and other metabolites) with GE_{li} - GE_{re} (effects mediated by siderophores alone). The strong positive correlation demonstrates that growth effects were mainly driven by siderophores and not by other secreted metabolites and residual nutrients. The black line and grey shaded area depict the best-fit trendline and the 95 % confidence interval of the linear regression (adjusted coefficient of determination R^2=0.755, n=2150 biologically independent rhizobacterial isolates, $F_{1,1248}$=6610 and two-side $P<2.2\times10^{-16}$ based on Student's t-test). **c**, The siderophore-mediated effects of the wild-type strains (producers) on the pathogen were representative of strong (*Pseudomonas aeruginosa*) and mild (*Burkholderia cepacia*) inhibition of the pathogen, while the siderophore-deficient isogenic mutants of both species completely lost their inhibitory effect under iron-limited conditions. Data represent the mean±s.d. of n=3 independent biological replicates (shown as black dots over the bars). **d**, The growth effect of purified pyoverdines of four *Pseudomonas* strains on pathogen under iron-limited condition were very similar to the effects of the raw supernatants (shown in brackets on X-axis). Data represent the mean±s.d. of n=4 independent biological replicates (shown as black dots over the bars).

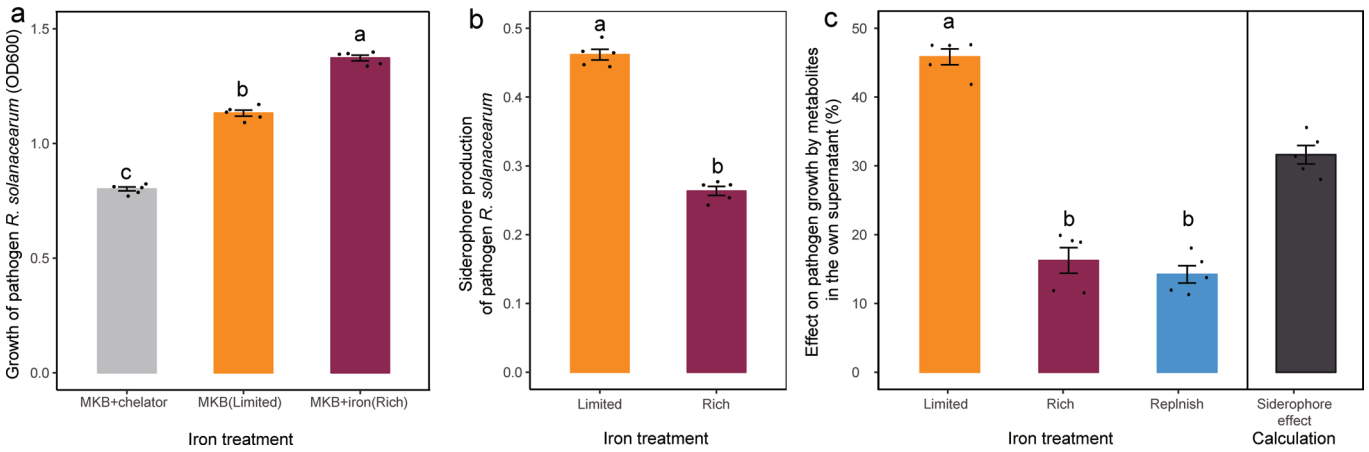

Extended Data Fig. 4 | *R. solanacearum* siderophore production and effects on its own growth. a, Iron deficiency constrains pathogen growth (after 48h growth measured as OD_{600}) in MKB medium (iron-limited) relative to MKB medium supplemented with 50 μM $FeCl_3$ (MKB+iron). Pathogen growth was even further reduced in MKB medium supplemented with 200 μM of the chelator 2,2'-Dipyridyl (MKB+chelator), which mimics the situation where the pathogen is exposed to a heterologous siderophore it cannot use. **b**, siderophore production of the pathogen *R. solanacearum* QL-Rs1115 under iron-limited and iron-rich conditions. **c**, The siderophores produced by the pathogen also promote its own growth under iron-limited conditions. The net effect caused by siderophores alone (right column, black symbols) was obtained by subtracting the growth effect of the iron-replenished supernatant (blue) from the growth effect of the iron-limited supernatant (yellow). Values indicate percentage fold-change in growth.In all panels, bars show the mean±s.d. based on 5 independent biological replicates (shown as black dots over the bars) and different lowercase letters above each bar represent significant differences based on analysis of variance (ANOVA) followed by Duncan's multiple range test ($P < 0.05$).

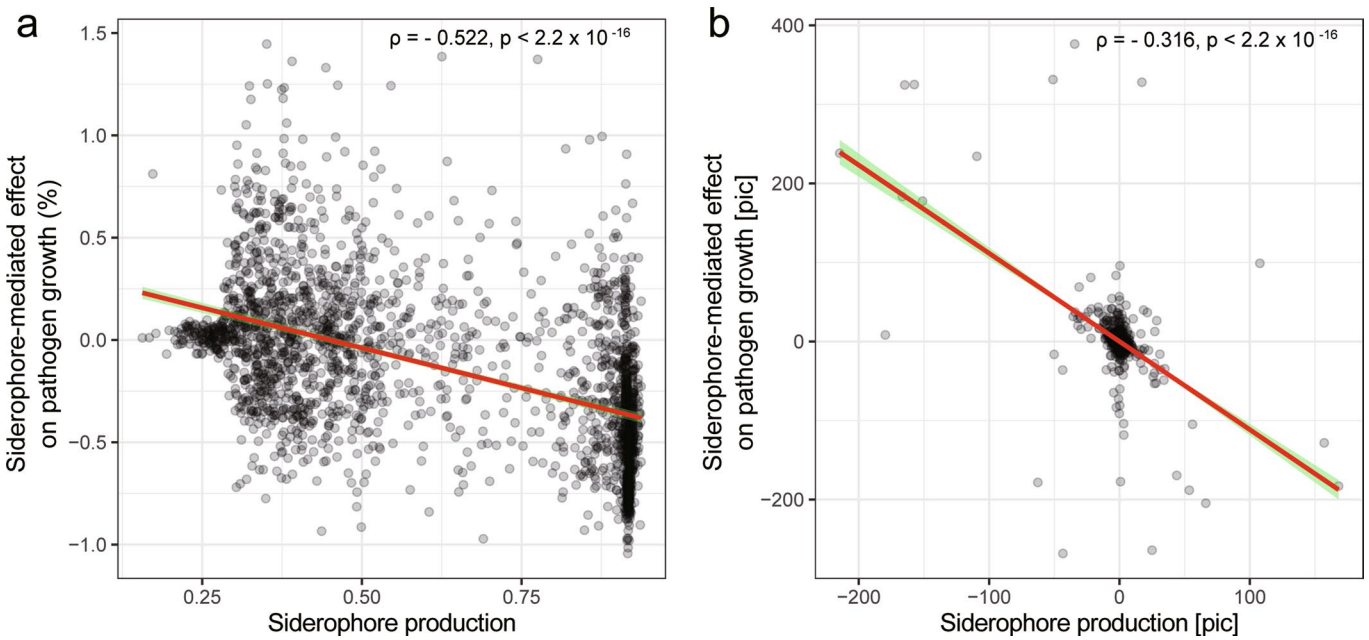

Extended Data Fig. 5 | The level of siderophore production scales negatively with siderophore-mediated effects on pathogen growth. a, The (phylogenetically uncorrected) values of siderophore production and siderophore-mediated effects on pathogen growth are negatively correlated. **b**, This correlation holds even after applying phylogenetically independent contrasts to both variables, showing that isolates producing high amounts of siderophores are generally more likely to inhibit *R. solanacearum* growth than isolates producing low amounts of siderophores. In both panels, black dots show values for each rhizosphere isolate (n=2150 biologically independent bacterial isolates). The correlation coefficients and p-values were obtained from Spearman rank correlations that account for the non-normal distribution of the phylogenetically corrected values. The red line and the green shaded area depict the best-fit trendline and the 95 % confidence interval of a linear regression, respectively.

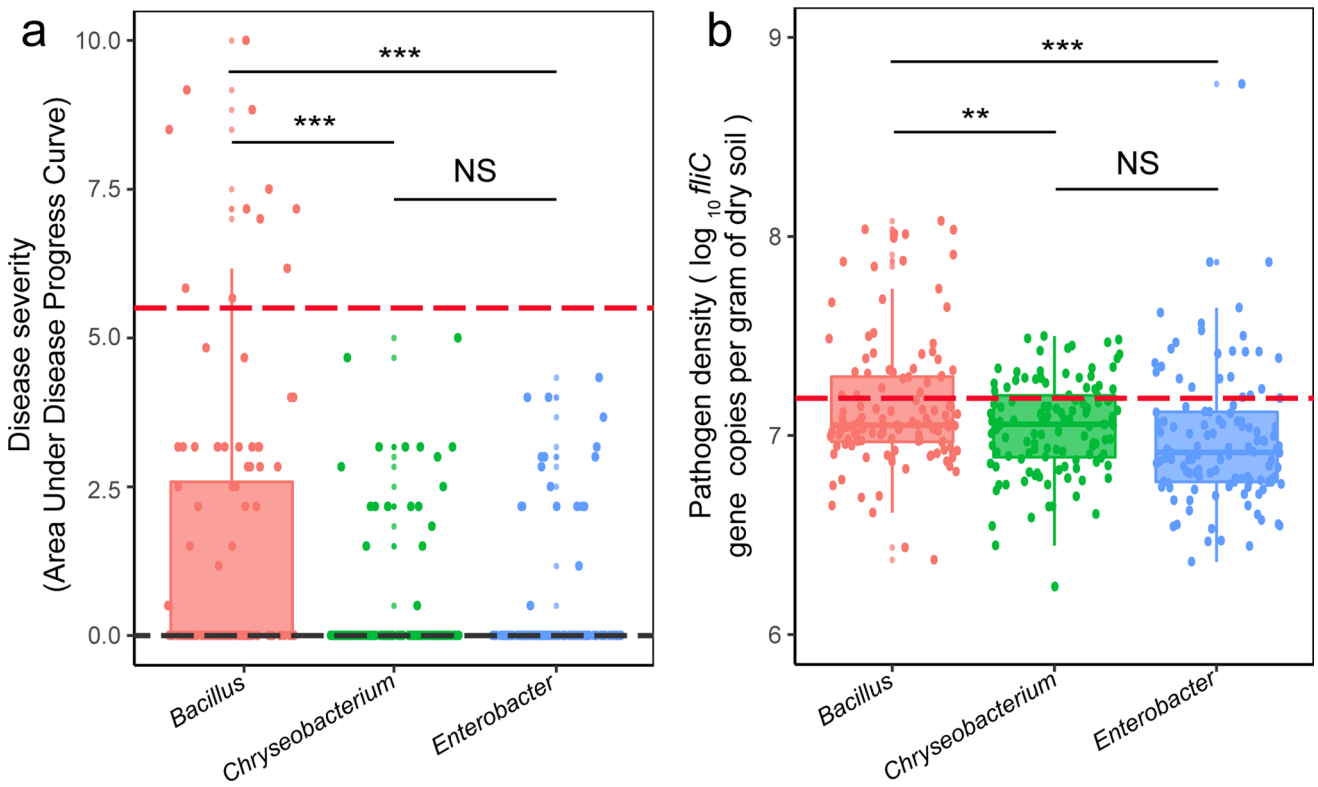

Extended Data Fig. 6 | Effect of siderophore-producing rhizosphere bacterial taxa on tomato plant disease incidence and pathogen density. a, The red dashed line shows the baseline level of disease incidence when soils were not pre-inoculated with rhizobacterial isolates and black dashed line represents results from the negative control treatment, where tomato plants were neither treated with rhizosphere bacteria nor with the pathogen. **b**, The red dashed line shows the baseline level of pathogen density when soils were not pre-inoculated with rhizobacterial isolates. In (**a**) and (**b**), box plots encompass the 25–75th percentiles, the whiskers extend to the minimum and maximum points and the midline indicates the median(n=360 biologically independent rhizobacterial isolates and *P* values were determined based on analysis of variance (ANOVA) followed by paired two-sided Student's *t* test). Significances for pairwise comparisons are (from left to right in) in (**a**): P=3.92×10^{-5}, P=4.87×10^{-5} and P=0.933, and in (**b**): P=0.004, P=0.0001 and P=0.116. NS represents non-significant difference (*$P < 0.05$, **$P < 0.01$, ***$P < 0.001$).

nature research

Corresponding author(s): Yangchun Xu and Zhong Wei

Last updated by author(s): Mar 23, 2020

Reporting Summary

Nature Research wishes to improve the reproducibility of the work that we publish. This form provides structure for consistency and transparency in reporting. For further information on Nature Research policies, see Authors & Referees and the Editorial Policy Checklist.

Statistics

For all statistical analyses, confirm that the following items are present in the figure legend, table legend, main text, or Methods section.

n/a	Confirmed	
☐	☒	The exact sample size (*n*) for each experimental group/condition, given as a discrete number and unit of measurement
☐	☒	A statement on whether measurements were taken from distinct samples or whether the same sample was measured repeatedly
☐	☒	The statistical test(s) used AND whether they are one- or two-sided *Only common tests should be described solely by name; describe more complex techniques in the Methods section.*
☒	☐	A description of all covariates tested
☒	☐	A description of any assumptions or corrections, such as tests of normality and adjustment for multiple comparisons
☐	☒	A full description of the statistical parameters including central tendency (e.g. means) or other basic estimates (e.g. regression coefficient) AND variation (e.g. standard deviation) or associated estimates of uncertainty (e.g. confidence intervals)
☐	☒	For null hypothesis testing, the test statistic (e.g. *F*, *t*, *r*) with confidence intervals, effect sizes, degrees of freedom and *P* value noted *Give P values as exact values whenever suitable.*
☒	☐	For Bayesian analysis, information on the choice of priors and Markov chain Monte Carlo settings
☐	☒	For hierarchical and complex designs, identification of the appropriate level for tests and full reporting of outcomes
☐	☒	Estimates of effect sizes (e.g. Cohen's *d*, Pearson's *r*), indicating how they were calculated

Our web collection on statistics for biologists contains articles on many of the points above.

Software and code

Policy information about availability of computer code

Data collection	No software was used for data collection
Data analysis	Most of the analyses were carried out using R version 3.1.2 using standard functions implemented in the base package; Adobe Illustrator version 23.0.1 was used for creating figures; Microsoft excel version 16.30 was used for data analysis. Mega version 7 and QIIME2 version 2018.11.0 were used to sequences analysis. Additional details are described in the Methods section.

For manuscripts utilizing custom algorithms or software that are central to the research but not yet described in published literature, software must be made available to editors/reviewers. We strongly encourage code deposition in a community repository (e.g. GitHub). See the Nature Research guidelines for submitting code & software for further information.

Data

Policy information about availability of data

All manuscripts must include a data availability statement. This statement should provide the following information, where applicable:

- Accession codes, unique identifiers, or web links for publicly available datasets
- A list of figures that have associated raw data
- A description of any restrictions on data availability

We deposited the following sequences at NCBI under the listed accession numbers: 2150 strains' sequences(MK823189-MK825338); Raw data of 80 soil samples' high-throughput sequences(SRR8949365-SRR8949444). All source data has been deposited to Dryad Digital Repository with the following digital identifier: https://doi.org/10.5061/dryad.p8cz8w9mb.

Field-specific reporting

Please select the one below that is the best fit for your research. If you are not sure, read the appropriate sections before making your selection.

☐ Life sciences ☐ Behavioural & social sciences ☒ Ecological, evolutionary & environmental sciences

For a reference copy of the document with all sections, see nature.com/documents/nr-reporting-summary-flat.pdf

Ecological, evolutionary & environmental sciences study design

All studies must disclose on these points even when the disclosure is negative.

Study description	We examined the ability of 2150 individual members of 80 rhizosphere microbiomes, covering all major phylogenetic lineages, to suppress the bacterium Ralstonia solanacearum, a global phytopathogen capable of infecting various crops, both in vitro and in vivo in controlled greenhouse experiments using tomato plants. We hypothesized that competition for iron, through the secretion of siderophores that scavenge iron from the environment, could represent a universal mechanism determining how strongly members of the soil microbiome can suppress the pathogen and protect plants.
Research sample	DNA from 80 rhizosphere soil samples 2150 bacterial isolates from 80 rhizosphere soil samples.
Sampling strategy	80 rhizosphere soil samples were collected from individual tomato plants located on four geographically distant fields that have suffered from bacterial wilt disease for 3-15 years. Twenty rhizosphere soil samples, corresponding each to an individual plant, were collected from each site. To this end, the excess soil was first gently shaken from the roots and the remaining soil attached to roots was considered as the rhizosphere soil. 32 isolates were randomly picked per rhizosphere soil sample. Only high dilutition samples were used for isolation to prevent potential fungal contaminants. Isolates were then re-streaked on TSA plates for colony purification. Approximately 16.0 % of bacterial isolates failed to grow on the TSA plates for unknown reasons and were omitted from the data set (approximately the same number of isolates failed to grow per each field). The final collection consisted of 2150 bacterial isolates from 80 rhizosphere soil samples. We used 16S rRNA amplicon sequencing to taxonomically identify all 2150 rhizobacterial isolates. we used Illumina sequencing to reveal the whole microbial community structure for each plant in a cultivation- independant way.
Data collection	SG, ZW, XW, ML and XM performed lab experiments and collected the data; SG, ZS, TY, KC performed greenhouse experiments and collected the data. (see methods for detail)
Timing and spatial scale	All samples were collected between march and december 2016
Data exclusions	No data exclusions
Reproducibility	All measurements were carried out in triplicate. The experimental sampling was repeated across four independent field sites separated by 500-1000 km to ensure full replication.
Randomization	32 bacterial isolates were randomly picked per rhizosphere soil sample. The sampling was randomized to ensure a balanced sample representation accross sites and plants. Samples were randomized during lab experiments, plants were randomized during greenhouse experiments (see methods).
Blinding	We used abstract labels for the different bacterial isolates during the lab and greenhouse experiments.

Did the study involve field work? ☒ Yes ☐ No

Field work, collection and transport

Field conditions	Agricultural fields in China,
Location	Changsha (112°58′ E, 28°11′ N), Ningbo (121°67′ E, 29°91′ N), Nanchang (115°51′ E, 28°41′ N), and Nanning (108°21′ E, 22°49′ N)
Access and import/export	The sample collection did not involve sensitive ecosystems. Minimal amounts of soil were collected at each sites (a few grams per sample)
Disturbance	No disturbance caused by this work.

Reporting for specific materials, systems and methods

We require information from authors about some types of materials, experimental systems and methods used in many studies. Here, indicate whether each material, system or method listed is relevant to your study. If you are not sure if a list item applies to your research, read the appropriate section before selecting a response.

Materials & experimental systems

n/a	Involved in the study
☒	☐ Antibodies
☒	☐ Eukaryotic cell lines
☒	☐ Palaeontology
☒	☐ Animals and other organisms
☒	☐ Human research participants
☒	☐ Clinical data

Methods

n/a	Involved in the study
☒	☐ ChIP-seq
☒	☐ Flow cytometry
☒	☐ MRI-based neuroimaging